



Linear and nonlinear optical studies of thermally evaporated chalcogenide a-Pb-Se-Ge thin films

Ahmed Saeed Hassanien^{a,b,*}, Ishu Sharma^c, Kamal A. Aly^{d,e}

^a Engineering Mathematics and Physics Department, Faculty of Engineering at Shoubra, Cairo, 11629, Benha University, Egypt

^b Physics Department, Faculty of Science and Humanities in Afif Governorate, Afif, 11921, Shaqra University, Saudi Arabia

^c Department of Physics, Amity University Dubai, Dubai, United Arab Emirates

^d Physics Department, Faculty of Science, Al-Azhar University, P.O. 71452, Assiut, Egypt

^e Physics Department, Faculty of Science and Arts Khulais, Jeddah University, Jeddah, Saudi Arabia

ARTICLE INFO

Keywords:

Glassy samples
Amorphous thin films
Optical characteristics
Optical energy gap
Refractive index dispersion
Non-linear optical parameters

ABSTRACT

This article is dedicated to studying optical characteristics of thermally evaporated $\text{Pb}_{10}\text{Se}_{90-x}\text{Ge}_x$ ($0.0 \leq x \leq 10.0$ at.%) thin films. These films were deposited on pre-cleaned high-quality glass substrates under a vacuum about 5×10^{-4} Pa. The amorphous nature of films was affirmed by X-ray diffractograms. Elemental analysis was done by Energy-dispersive X-ray spectroscopy. Optical properties of Pb–Se–Ge films were studied and investigated using the transmission spectra. Thickness of the films and refractive index were computed utilizing Swanepoel envelope method. Wemple-Di-Domenico model was applied to get dispersion energies and oscillator parameters. Absorption coefficient values of films were estimated and found to be of the order of 10^{-4}cm^{-1} . The electronic transitions of a-Pb₁₀Se_{90-x}Ge_x thin films were resulted from allowed indirect transitions and the optical band gap was found to decrease from 1.623 eV to 1.538 eV with increasing Ge-ratio while Urbach energy was found to increase from 61 meV to 86 meV. All discussed parameters strongly depend on the Ge-concentration.

1. Introduction

The semiconductor industry is continuously innovating itself to expand the possibility in science and technology as per the current industry need. Hence, nano-dimensional chalcogenides of bulk and thin-film materials have a specific forte in semiconductor manufacturing and are still studied for use in many potential industrial applications [1–4]. Chalcogens have a broad transparency window in the infra-red region, with high photosensitivity, linear and non-linear index of refraction value, high quantum efficiency and low phonon energy. Hence, are widely used in switching devices, waveguides, reversible phase change materials, NIR-window, IR camera, photovoltaic, holography, etc. [5–8]. Glassy chalcogenide materials are described by the existence of homopolar bonds, localized states, short-range order, and different kinds of imperfections. Therefore, their properties such as electrical, optical, and physical can be tailored, engineered, and tuned in Refs. [9–12].

In addition, relatively easy synthesis of chalcogen glassy alloys reduces the production cost. More to this, the chemical composition can be

easily varied, according to the requirement. This opens the possibility of creating complex optical systems, for example, optical computers, sensors, compact optical devices, light sources, biological sensors, etc. using chalcogens [13–15]. Among chalcogenide glasses, Se and Te are the majorly used chalcogens in the material industry but have many limitations in their pure form [16]. The Te-based glasses have a broad transparency window and are used majorly in phase change materials, but Te crystallizes very easily and therefore, its glass-forming ability is very low.

Even pure Se is a very good glass former and used in broad industrial applications, but also has shortcomings like a low sensitivity and lifetime. These shortcomings can be overcome by the addition of some other element having the same electronegativity. Mostly chalcogens are p-type semiconductors and the Fermi level in each is pinned. It has been seen that the addition of metallic additives such as Pb, Sb, Bi alters the concentration of valence alteration pairs (positively and negatively charged defect states), unpins the Fermi level and hence results in p to n type carrier reversal and properties can be controlled [17–19].

In previous works, the influence of adding Bi and Sb to the

* Corresponding author. Engineering Mathematics and Physics Department, Faculty of Engineering at Shoubra, Cairo, 11629, Benha University, Egypt.

E-mail addresses: a.s.hassanien@gmail.com, ahmed.hassanien@feng.bu.edu.eg (A.S. Hassanien), ishuphy@gmail.com, isharma@amityuniversity.ae (I. Sharma), kamalaly2001@gmail.com (K.A. Aly).

<https://doi.org/10.1016/j.physb.2021.412985>

Received 14 January 2021; Received in revised form 2 March 2021; Accepted 11 March 2021

Available online 17 March 2021

0921-4526/© 2021 Elsevier B.V. All rights reserved.

germanium, selenium, and tellurium based glassy matrix has already been studied [19–21]. Therefore, in the present manuscript, $Pb_{10}Se_{90}$ is chosen as a parent network. Due to the comparative size and electronegativity values of lead and selenium, a high quality covalent binary alloy is obtained [22].

Lead element, Pb has a high refractive index, and therefore, Pb based glassy matrix becomes a platform for many next-generation image processing applications [23]. In addition, also opens a possibility of creating optical system such as sensors, coupling elements etc. The laser diode based on Pb, are important source for tuneable emission in Mid-IR region [24].

To customize the properties, the third element added is Ge and is associated with the change in optical and electrical constants. Glasses of Ge_xSe_{1-x} are also among the best covalent glass formers and is a broadly studied framework. The authors have already discussed the physical and optical properties of several studies related to Ge–Se glassy alloys, thoroughly [12,17–20]. It has been seen that alloying of Se with Ge improves the glass thermal stability, in terms of the glass transition temperature, resistivity, and reduces the ageing effect [25,27,28]. The transparent window also expands with Ge addition in the IR domain. Selenium and germanium cross-links modify the bond and give strength to the system average bond, which results in good chemical stability. Even the size compatibility of all the constituent results in an excellent quality alloy for various usage [17,20]. It has been seen that with Pb addition in Ge based glasses, a majority of carrier type reversal takes place. Pb based Ge glasses have a potential application in thermoelectric and photovoltaic devices, as Pb alters the charged defects states [25,26]. Moreover, with small band gap value and large Bohr radius, Pb based Ge–Se glasses have potential applications in photodetector, solar cells, chemical as well as biological sensors [26–28].

Therefore, in this manuscript, the study is based on optical properties of the $Pb_{10}Se_{90-x}Ge_x$ system with $x = 0.0, 2.5, 5.0, 7.5, \text{ and } 10.0$ at. %, where Se-element is being substituted by Ge-element. The addition of Ge may result in new defects and consequent alteration in physical and optical properties. The motivation behind this work is firstly to manufacture good quality films of $Pb_{10}Se_{90-x}Ge_x$ with high-homogeneity via the vapor deposition process. Secondly, the authors through this work, seek to study the optical characteristics of $Pb_{10}Se_{90-x}Ge_x$ thin films based on optical transmission measurements only, using the Swanepoel method.

This work also aims to study the refractive index dispersion and explore the effective single oscillator model and the dispersion energies of the system. The authors also studied coefficient of absorption, optical bandgap, Urbach energy of $a-Pb_{10}Se_{90-x}Ge_x$ films and the relationship between them. Furthermore, and based on the experimental bandgap energy values, some nonlinear optical parameters were also evaluated. Table 1 reports some physical properties, such as Band-gap energy (E_g), ionization energy (E_{ion}), electron affinity (E_{EA}), electronegativity (η), bond energy, E_B , and the coordinated number (N_C), of the compositional elements of the ternary $Pb_{10}Se_{90-x}Ge_x$ samples [7,29–31].

2. Experimental methodology

2.1. Samples preparation

For synthesizing the bulk glassy $Pb_{10}Se_{90-x}Ge_x$ samples ($x = 0.0, 2.5,$

Table 1
Some physical parameter values of the compositional elements of amorphous $Pb_{10}Se_{90-x}Ge_x$ samples [7,29–31].

Element	E_g (eV)	(E_{ion}) (eV)	(E_{EA}) (eV)	η (Pauling scale)	E_B (kJ/mol)	N_C
Pb	0.00	7.41	0.36	2.33	86.61	4
Se	1.74	9.75	2.02	2.55	184.09	2
Ge	0.67	7.9	1.23	2.01	157.62	4

5, 7.5, 10.0 at. %) a melt quench technique was used. High purity (5 N) elements were weighed as per at. weight %-age. The weighed materials were then sealed in evacuated quartz ampoules using a diffusion pump to a residual pressure of approximately 10^{-4} Pa. These ampoules were heated a rocking furnace to a temperature of 1100 °C. The furnace heating rate was kept at 2–3 °Cmin⁻¹ and a step heating process was followed. The applied step-heating was done at 300 °C, 500 °C, 700 °C, 900 °C and 1000 °C, each step was continued for 1 h. Before the sudden quenching of the $Pb_{10}Se_{90-x}Ge_x$ molten in the ice water, the sealed ampoules were left in the oven at 1100 °C for 18 h with continuing at shake. The continuous rocking and step heating process is adopted to ensure the proper homogeneity of the molten mixture. The ingots bulk materials were taken out from the quenched ampoules, for use in the different characterization equipment. Where, the crushed form of glassy alloys was used for XRD, EDAX and SEM studies, as well as to synthesize the film samples.

The film samples were fabricated using the physical vapor deposition technique, employing the coating unit of Denton-Vacuum (*DV Model 502 A*). The deposition of the ternary $a-Pb_{10}Se_{90-x}Ge_x$ thin films was carried out using a Molybdenum boat. Before the deposition process, a heavy current has been passed through this boat, until it becomes flashy red hot. This step was achieved to remove any impurities may be existed in the boat or for the pre-cleaning purpose. The prepared non-crystalline $Pb_{10}Se_{90-x}Ge_x$ thin films have been deposited at room temperature and under a vacuum of about 5×10^{-4} Pa on colorless, high-quality KH-microscopic glass slides. These glass sheets have been cleaned ultrasonically by double-distilled water, acetone followed by ethyl alcohol, and then oven dried at a temperature of 100 °C finally. Film thicknesses and evaporation rate were continuously monitored and fixed at ≈ 800 nm and 10 nm/s, respectively. The monitoring and controlling of these parameters were done with a quartz crystal, Denton's monitor of Model *DTM-100*, positioned close to the substrate.

2.2. Characterizations of $Pb_{10}Se_{90-x}Ge_x$ samples

X-ray diffraction (XRD) technique using (*Philips diffractometer 1710*) was used to confirm the amorphous behavior of $Pb_{10}Se_{90-x}Ge_x$ bulk alloys and films. This diffractometer has a Copper target and Ni filter with the wavelength, $\lambda = 1.542$ Å. The elemental analysis of films composition was done using Energy dispersive X-Ray Spectroscopy, EDAX-technique using (*Link analytical EDS*) at different spots in the film. The measured error of an individual element in the composition fall within the range of $\pm 1.0\%$. The normal incidence transmission spectra, T of $Pb_{10}Se_{90-x}Ge_x$ film samples were obtained by double beam UV–Visible–NIR spectrophotometer (*2101–UV–VIS*) in the range $0.5 - 2.5 \mu\text{m}$ of wavelength. All-optical measurements and the samples' characteristics were performed at room temperature. The used spectrophotometer is equipped with a slit of width is about 1 nm and is extremely smaller than line width. Therefore, slit width correction is not required.

Swanepoel envelope method was used to compute the thickness and refractive-index of $Pb_{10}Se_{90-x}Ge_x$ thin-film using the obtained transmission spectra [32,33]. An envelope was created on the transmission spectra of the amorphous $Pb_{10}Se_{90-x}Ge_x$ films, to know the maximum (T_M), minimum (T_m) and the average values of these spectra at the wavelength corresponding to the interference fringes. These T_M , T_m envelopes have been plotted around the extreme for each transmission spectrum, and the computations were done using *OriginPro 2019b* software program [34–36].

3. Results and discussion

3.1. Samples identifications

Fig. 1 illustrates the X-ray diffractograms of the ternary $Pb_{10}Se_{90-x}Ge_x$ films at different Ge-percentages. As shown in the figure no

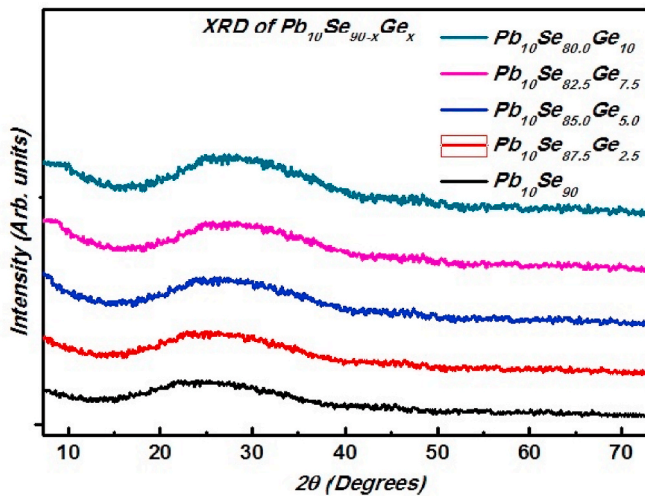


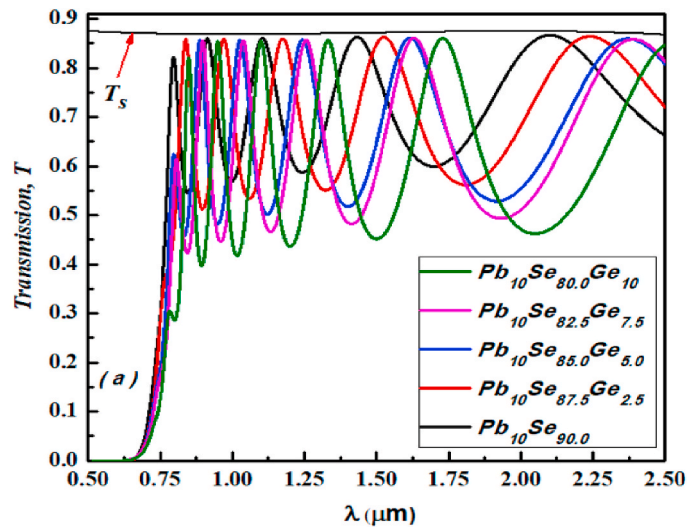
Fig. 1. X-ray spectra of the ternary $Pb_{10}Se_{90-x}Ge_x$ films at different Ge percentages.

diffraction sharp peaks were detected. The absence of any diffraction lines confirms the non-crystallinity of the synthesized Pb–Se–Ge films.

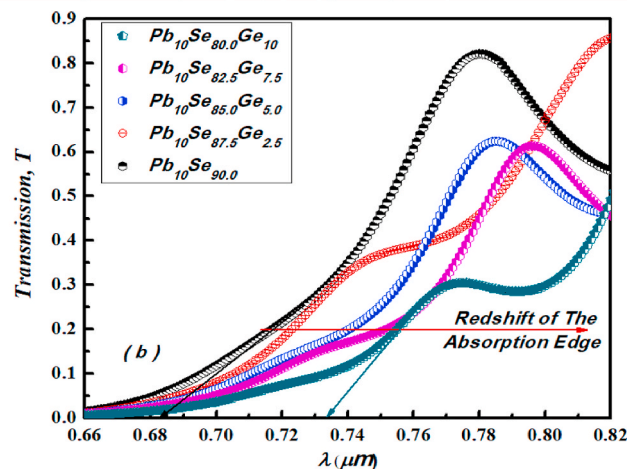
However, the XRD curves show one stepped hump at the diffraction position on $(2\theta) \approx 20^\circ\text{--}35^\circ$ owing to the amorphous nature of the glass substrate [23,26,37]. The surface of the samples was scanned using the EDAX technique to detect the atomic percentage of the individual component elements for each film sample. The obtained results confirm that the ratios of the elements detected experimentally are within an error range of $\pm 1.0\%$. For more accuracy, each film sample has been scanned several times and in different positions, and the average value was accounted. The EDAX results did not illustrate here as they have been published elsewhere [38].

3.2. Optical properties

The study of optical characteristics of materials is very crucial to judge the possibility of using this material in optoelectronic, photovoltaic applications and devices. Optical studies range from studying the absorption of material, its transmittance, and its reflectance for electromagnetic waves, to knowing the bandgap, the dispersion energies, electronic transitions, etc. Therefore, the following section covers detailed discussion on the optical properties of the non-crystalline



a: Transmission spectrum of $Pb_{10}Se_{90-x}Ge_x$ films ($x = 0, 2.5, 5.0, 7.5$ and 10.0 at. %).



b: Red-shift of the absorption edge of films as the Ge-ratio increased.

Fig. 2. a: Transmission spectrum of $Pb_{10}Se_{90-x}Ge_x$ films ($x = 0, 2.5, 5.0, 7.5$ and 10.0 at. %). Fig. 2-b: Red-shift of the absorption edge of films as the Ge-ratio increased. (For interpretation of the references to color in this figure legend, the reader is referred to the Web version of this article.)

Pb₁₀Se_{90-x}Ge_x film samples.

3.2.1. Optical transmission spectra

Optical transmission (T) indicates the percentage of light transmitted through a clear optical material. Some applications, like optical fiber connections, optoelectronic sensors, and Photonics need that the used material must have a higher level of transmission. The transmission spectra of a certain film sample are affected by the coating process and its applied conditions, the thickness of the film, the film material itself, and the used substrate, etc. For semiconductor films, the transmission of a glazing film range between 90% of the highest transparent films to about 40% of highly coating materials. This range varies depending upon the film sample and its substrate.

Fig. 2-a illustrates the transmission spectra of the a-Pb₁₀Se_{90-x}Ge_x thin films. Five distinguished interference fringes, with peak maxima at 0.87 and minima at 0.45 approximately, are clearly observed in the transmission spectra. The fabricated film thickness is about 800 nm, which subsequently results in a greater number of fringes. As the increase in film thickness increases the number of interference fringes [39]. The interference fringes begin at the end of the visible region and the start of the near-infrared region.

It can also see from Fig. 2-a that there is a strong absorption by films at the wavelength ranges between 0.7 and 0.9 μm, where the absorption-edge of the films is observed. The intensity of the interference fringes decreases and almost reaches zero at the absorption edge. Fig. 2-b shows the observed absorption edge, and a red-shift is observed from 0.683 to about 0.735 μm with the increase in Ge content. Ge addition increases the strength of the interconnection between the film atoms. When Ge enters the system, it forms heteropolar bonds with Se with the bond energy of 49.44 kcal/mol. Therefore, the number of Se-Se homopolar bond decreases, bond energy with the bond energy of 44.00 kcal/mol. Also, heteropolar bonding strength is stronger than homopolar bonds [30,31].

Moreover, Ge-element has a lower band-gap energy ($E_g = 0.67$ eV) as compared to Se ($E_g = 1.74$ eV). Therefore, adding the Ge-element increases the absorption of the film samples and results in the redshift of the absorption edge. The wavelengths corresponding to the position of the absorption edges of all films are shown in Fig. 2-b.

Fig. 3 also shows the transmission spectra of a-Pb₁₀Se₉₀ (as reference), to depict the maximum, minimum and glass substrate transmission interference values, T_M , T_m and T_s , respectively. The average transmission value of the films, T_α can be obtained as the geometric mean value of both of T_M and T_m ; i.e. $T_\alpha = (T_M T_m)^{0.5}$ [40]. Fig. 3 also

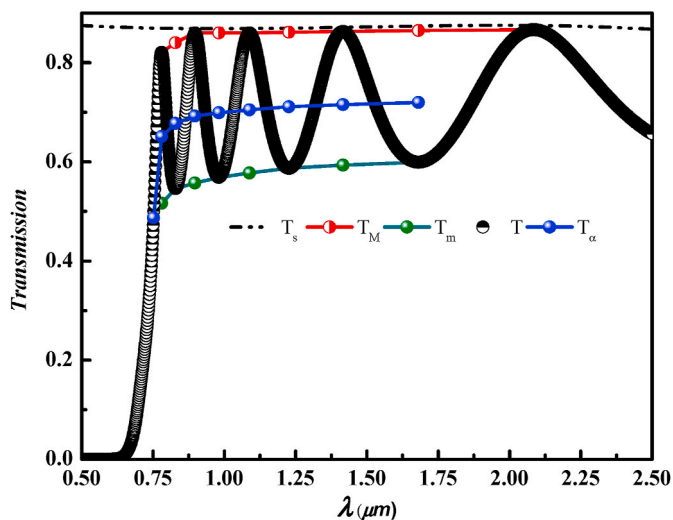


Fig. 3. Transmission spectra, transmission envelope values; T_M , T_m and T_α of Pb₁₀Se₉₀ thin films.

shows that the first-order interference peak exhibited at a wavelength, $\lambda \approx 0.760$ μm and is known as the absorption edge. It is shown from the figure that almost all the fringes have maxima except the first fringe. The calculated T_M , T_m and d values corresponding to ($x = 0, 2.5, 5.0, 7.5$ and 10.0 at. %) are tabulated in Table 2.

3.2.2. Refractive index evaluation

The refractive index (n) and thickness (d) and the of Pb₁₀Se_{90-x}Ge_x thin films are determined using the Swanepoel envelope method [32, 33]. Based on Manificier et al. to estimate the optical constants and film thickness [41]. The refractive index, n_1 can be determined using the following form [39,40]:

$$n_1 = \sqrt{\left[N + \sqrt{N^2 - S^2} \right]} \quad (1)$$

Where:

$$N = 2S \left(\frac{T_M - T_m}{T_M \times T_m} \right) + \left(\frac{S^2 + 1}{2} \right) \quad (2)$$

Here (S) is the refractive index of glass substrate obtained from its transmission spectra [38,42]:

$$S = \frac{1}{T_s} + \sqrt{\left(\frac{1}{T_s^2} - 1 \right)} \quad (3)$$

The calculated n values (using equations (2) and (3), then substitute in Eq. (1)) are given in Table 2. The precision of these n values can be improved by computing the film thickness using basic interference Eqs.:

$$2nd = m_o \lambda \quad (4)$$

Here the order number (m_o) is equal an integer (i.e. 1, 2, 3, ...) for each maximum and a half integer (1/2, 3/2, 5/2, ...) for each minimum in the transmission spectra. To the first approximation the film thickness, d_1 is given as:

$$d_1 = \lambda_1 \lambda_2 / (2n_2 \lambda_1 - 2n_1 \lambda_2) \quad (5)$$

Here, λ_1 , and λ_2 are two adjacent maxima (or two adjacent minima) wavelength values and n_1 and n_2 are respective refractive index. Using d_1 -and n -values in Eq. (4), the m_o values are calculated for all maxima or minima fringes. Using the accurate m_o -values, the $d_{corrected}$ values can be calculated and the tabulated in Table 2.

Furthermore, an easy graphical route has been used to derive the number of the first order (m_1) and the film thickness (d) based on Eq. (1). Then, Eq. (4) can be reformulated as follows [42–44]:

$$l/2 = 2d(n/\lambda) - m_1 \quad (6)$$

Here, m_1 represents the first-order value. It is equal to an integer for any maximum (1, 2, 3, ...) and a half-integer for any minimum (1/2, 3/2, 5/2, ...), while (l) takes the values 0, 1, 2, 3, Consequently, from a graph plot between ($l/2$) and (n/λ), a straight line intersects the ordinate at a value equals ($-m_1$) and its slope is ($2d$).

Fig. 4 shows the graphical dependence of ($l/2$) upon (n/λ). Thereby, the thickness (d) and the first-order value (m_1) of Pb–Se–Ge amorphous thin films can be obtained. According to the figure, the obtained thickness values are 797.5, 804, 807, 776 and 784 nm for the amorphous Pb₁₀Se_{90-x}Ge_x films, where $x = 0.0, 2.5, 5.0, 7.5$ and 10.0 at. %, respectively. Fig. 4 confirms also the computed values tabulated in Table 2.

Therefore, the film thickness taken from quartz monitor and computed from the Swanepoel envelope method is found in good agreement. Furthermore, using the computed values of refractive index from Table 2 and performing the least-square fitting as per Cauchy-dispersion relation, which is given as:

$$n(\lambda) = A + \frac{B}{\lambda^2} \quad (7)$$

Table 2The refractive index and thickness values of the amorphous $\text{Pb}_{10}\text{Se}_{90-x}\text{Ge}_x$ film samples using the envelope Swanepoel route.

Sample	λ	T_M	T_m	T_s	n	$d(\text{nm})$	m_o	M	$d_{\text{corr}}(\text{nm})$	n_{corr}	
Pb10Se90	1681	0.86	0.60	0.87	2.64	–	2.561	2.50	797	2.64	
	1416	0.86	0.59	0.87	2.67	793	3.075	3.00	796	2.67	
	1226	0.86	0.59	0.87	2.70	793	3.590	3.50	796	2.70	
	1088	0.86	0.58	0.87	2.73	798	4.101	4.00	796	2.73	
	981	0.86	0.57	0.87	2.77	800	4.611	4.50	796	2.77	
	897	0.86	0.56	0.87	2.82	792	5.126	5.00	796	2.82	
	829	0.84	0.55	0.87	2.83	918	5.570	5.50	806	2.86	
	d1 = 816, $\delta 1 = 50$ nm 6.30%, d2 = 798, $\delta 1 = 3.56$ nm (0.45%)										
Pb10Se87.5Ge2.5	1792	0.86	0.56	0.87	2.78	–	2.51	2.50	804	2.78	
	1509	0.86	0.55	0.87	2.81	770	3.04	3.00	798	2.81	
	1307	0.86	0.551	0.87	2.84	857	3.51	3.50	806	2.84	
	1158	0.86	0.54	0.87	2.88	798	4.02	4.00	805	2.88	
	1043	0.86	0.53	0.87	2.91	807	4.52	4.50	805	2.92	
	953	0.86	0.52	0.87	2.96	802	5.02	5.00	805	2.96	
	881	0.86	0.51	0.87	3.01	816	5.52	5.50	806	3.01	
	d1 = 808, $\delta 1 = 29$ nm 3.50%, d2 = 804, $\delta 1 = 3.1$ nm (0.40%)										
Pb10Se85Ge5	1899	0.86	0.53	0.88	2.94	–	2.46	2.50	807	2.94	
	1599	0.86	0.52	0.87	2.96	828	2.95	3.00	811	2.97	
	1384	0.86	0.52	0.87	2.98	827	3.43	3.50	813	3.00	
	1227	0.86	0.51	0.87	3.03	795	3.93	4.00	811	3.04	
	1105	0.86	0.50	0.87	3.07	810	4.42	4.50	811	3.08	
	1010	0.86	0.49	0.87	3.12	794	4.92	5.00	809	3.13	
	933	0.86	0.47	0.87	3.22	698	5.49	5.50	797	3.18	
	870	0.86	0.46	0.87	3.27	817	5.98	6.00	799	3.23	
	d1 = 796, $\delta 1 = 45.25$ nm 5.70%, d2 = 807, $\delta 1 = 6.29$ nm (0.80%)										
	Pb10Se82.5Ge7.5	1915	0.86	0.49	0.88	3.08	–	2.51	2.50	776	3.08
1613		0.86	0.49	0.87	3.12	775	3.01	3.00	776	3.12	
1397		0.86	0.48	0.87	3.15	779	3.51	3.50	776	3.15	
1239		0.86	0.47	0.87	3.20	757	4.03	4.00	774	3.19	
1116		0.86	0.46	0.87	3.26	752	4.55	4.50	771	3.24	
1021		0.86	0.45	0.87	3.29	813	5.02	5.00	775	3.29	
943		0.85	0.45	0.87	3.33	819	5.50	5.50	779	3.34	
880		0.85	0.43	0.87	3.40	755	6.02	6.00	777	3.40	
d1 = 778, $\delta 1 = 27.6$ nm 3.55%, d2 = 776, $\delta 1 = 2.45$ nm (0.31%)											
Pb10Se80Ge10	2034	0.86	0.46	0.88	3.24	–	2.50	2.50	786	3.24	
	1713	0.86	0.45	0.87	3.30	747	3.03	3.00	779	3.28	
	1483	0.86	0.44	0.87	3.36	737	3.56	3.50	773	3.31	
	1315	0.86	0.44	0.87	3.37	833	4.04	4.00	780	3.35	
	1185	0.86	0.44	0.87	3.39	855	4.50	4.50	787	3.40	
	1083	0.85	0.43	0.87	3.43	800	4.99	5.00	789	3.45	
	1000	0.85	0.42	0.87	3.48	806	5.48	5.50	790	3.51	
	933	0.85	0.41	0.87	3.57	729	6.02	6.00	785	3.57	
	d1 = 787, $\delta 1 = 49.61$ nm 6.31%, d2 = 784, $\delta 1 = 6.35$ nm (0.80%)										

Therefore, Cauchy's parameters **A** and **B** are calculated. These parameters can be estimated by plotting $n(\lambda)$ versus $(1/\lambda^2)$ from the interception part and the slope of the linear portion. Using the values of Cauchy's parameters in equation (7), refractive index from 0.5 μm to 2.5 μm is calculated [39–43].

Fig. 5 shows the spectral dependence of **n** for all the film samples in the spectral range of 0.5 μm –2.5 μm . Refractive index values computed using Swanepoel envelope method are shown by solid symbols, whereas the refractive index values calculated using Cauchy's dispersion relation are shown by hollow symbols. A normal dispersion behavior is seen in refractive index values up to about 1.6 μm , the values decrease sharply and thereafter shows almost invariant behavior. Also, **n**-values are increasing with the addition of Ge in the system. Generally, these obtained results are in good agreement with a previous literature [1,45]. The relative errors in determining both (**n**) and ($\Delta n/n$), are typically like that of the transmission ($\Delta T/T$), which is within $\pm 1\%$.

3.2.3. Dispersion energies and related parameters

The single effective oscillator model proposed by Wemple–DiDomenico (**WDD model**) successfully explains the refractive-index dispersion and its ability to precisely deduce the dispersion energies and parameters [32–34]. The WDD model links the refractive index of a material with its effective single oscillator (E_o) and the dispersion energy (E_d). Moreover, these two energies are independent of each other, because of the energy E_d is dependent on the dielectric loss,

while E_o is not. Many optical parameters such as the band-gap energy, the oscillator strength (**f**), the lattice dielectric constant (ϵ_L), the static refractive index (n_o), and the moments M_{-1} , M_{-3} can be deduced using E_o and E_d -values.

The equation of single effective oscillator model is given as in this formula [32,33]:

$$(n^2 - 1)^{-1} = \frac{(E_o^2 - (h\nu)^2)}{(E_d E_o)} \quad (8)$$

Here, $h\nu$ represents the incident photon energy. Thereby, plotting a graphical relation between $(n^2-1)^{-1}$ vs $(h\nu)^2$, a straight line is obtained and its slope is equal to $(E_d E_o)^{-1}$ and the intercept on y-axis is equal to (E_o/E_d) . Such graphical illustration is shown in Fig. 6, and consequently, the two energies (E_d and E_o) values are computed and tabulated in Table 3.

The dispersion energy value (E_d) increases from 18.182 eV to 24.839 eV, while the energy of the single oscillator (E_o) decrease from 3.222 eV to 2.779 eV. The single oscillator energy is evaluated as twice the value of the optical band-gap energy as suggested by Tanaka (1980) [46]. Therefore, the band gap energy (E_g) values can also be obtained (Table 3). As observed the energy gap, E_g decreases as Ge-content increases. The increased disorder leads to the formation of localized states in the forbidden band gap, E_g , which further results in shrinkage of forbidden gap width, as observed from the E_o and E_g values (Table 3).

The oscillator strength (**f**), lattice dielectric constant (ϵ_L), and the

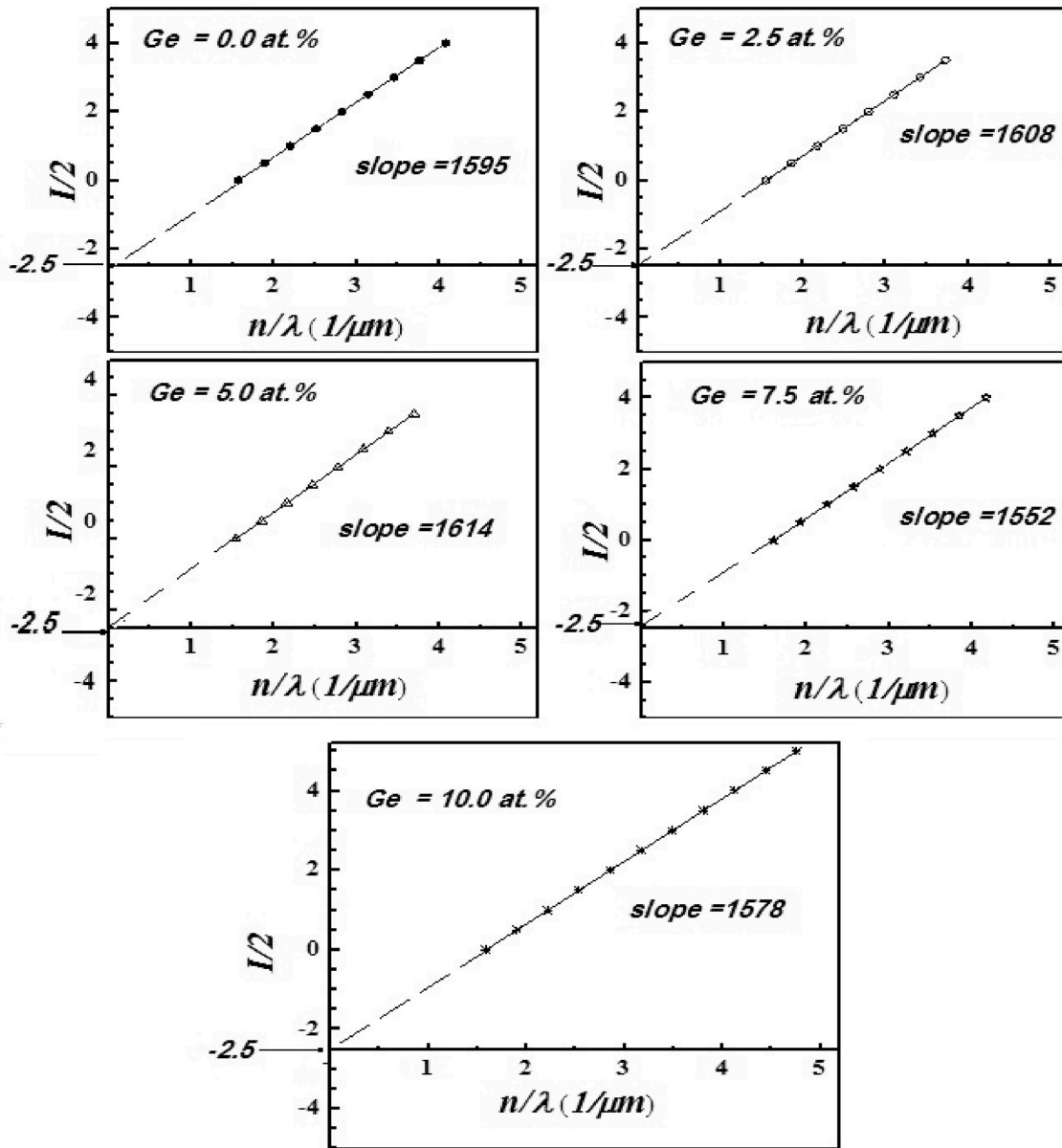


Fig. 4. The dependence of $(I/2)$ upon (n/λ) to estimate the thickness (d (nm) = slope/2) and the first-order value (m_1) of a-Pb₁₀Se_{90-x}Ge_x amorphous films.

static refractive index (n_o) are calculated as follows [39,50]:

$$f = E_d \times E_o, \quad \epsilon_L = 1 + \frac{E_d}{E_o} \quad \text{and} \quad n_o = \sqrt{1 + \frac{E_d}{E_o}} \quad (9)$$

While the moments M_{-1} , and M_{-3} can also be computed from the estimated E_o and E_g values by these Eqs. [50].:

$$E_o^2 = \frac{M_{-1}}{M_{-3}} \quad \text{and} \quad E_d^2 = \frac{M_{-1}^3}{M_{-3}} \quad (10-a)$$

After re-arranging, they become:

$$M_{-1} = \frac{E_d}{E_o} \quad \text{and} \quad M_{-3} = \frac{M_{-1}}{E_o^2} \quad (10-b)$$

These computed optical parameters (f , ϵ_L , n_o , and the moments M_{-1} and M_{-3}) (Table 3) increases as the Ge-content increases. The Ge addition results in increased localized states, which further leads to the decrease in the band-gap width and the optical bandgap energy. The band-gap energy is inversely proportional to the refractive index, therefore, the increase in the Ge-content leads to the increase in the

refractive index values which in turns leads to the increase in the oscillator strength (f), the lattice dielectric constant (ϵ_L), the dispersion energy (E_d) and static refractive index (n_o) and the moments. Few literature studies also report the similar results such as El-Nahass et al. (2008) for Ge_{1-x}Se₂Pb_x films [51] and Deepika et al. for Se₅₈Ge₃₆Pb₆ thin films [52].

There is another substantial implementation of the WDD model. Where it links the dispersion energy and some essential optical parameters such, the effective coordination number of the cation (N_c), the effective number of valence electrons/anion, and the chemical valency of the anion (Z_a). The Eq. that link between these parameters is given as follows [39,46,53,54]:

$$E_d = \beta \times N_c \times Z_a \times N_e \quad (11)$$

Here, β is a constant. For the ionic materials $\beta_i = 0.26 \pm 0.03$ eV, while for the covalent materials it is $\beta_c = 0.37 \pm 0.04$ eV [39,55]. For all the films under investigation, the effective coordination number is equal to 4 and hence, N_e can be calculated. For the thin film sample Pb₁₀Se₉₀:

$$N_e = (4 \times 10 + 6 \times 90)/90 = 6.44$$

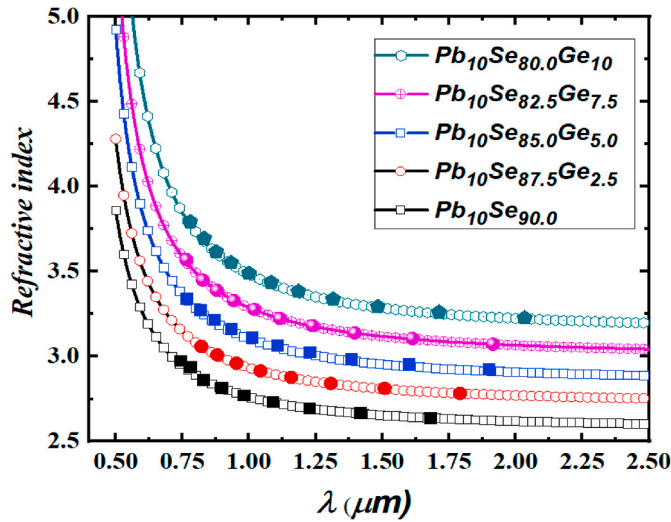


Fig. 5. Illustration of the refractive index dispersion of the present films. The solid points exhibit the estimated values in accordance with Cauchy's dispersion Eq.

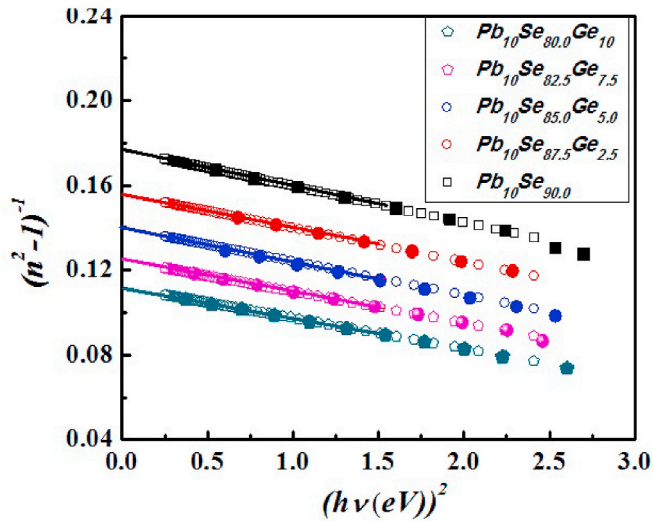


Fig. 6. The variation of $(n^2 - 1)^{-1}$ with the square of the photon energy $(h\nu)^2$ for a-Pb₁₀Se_{90-x}Ge_x thin films ($x = 0.0, 2.5, 5.0, 7.5$ and 10.0 at %) thin films.

$$Z_a = 2 \text{ Thus, } E_d = 19.08 \text{ eV.}$$

And even for the film sample Ge_{2.5}Pb₁₀Se_{87.5}:

$$N_e = (4 \times 2.5 + 4 \times 10 + 6 \times 87.5) / (8.75) = 6.57$$

$$Z_a = 2 \text{ and } E_d = 19.45 \text{ eV.}$$

Therefore, the theoretical value of $E_d(\text{th})$ in eV are estimated for Pb₁₀Se_(1-x)Ge_x thin-film samples, and listed in Table 3, too. The obtained values are found to be in good consistency with the values obtained from the single effective oscillator model. Also, the refractive index (n) depends upon the photon wavelength(λ), the high frequency dielectric-constant (ϵ_∞) and carrier concentration per effective mass (N/m^*) as per the following expression [5,39,40]:

$$n^2 = \epsilon_\infty - \left(\frac{e^2}{4\pi^2 c^2 \epsilon_0} \right) \left(\frac{N}{m^*} \right) \lambda^2 \quad (12)$$

Here (e) is the charge of an electron, (ϵ_0) is the space permittivity and (c) is the speed of the light. Therefore, plotting a graph between (n^2) (on the ordinate) and (λ^2) (on the abscissa), a straight line is obtained (Fig. 7). The y-intercept gives the value of ϵ_∞ and the slope equals to

Table 3

The computed results of the linear and nonlinear optical parameters of Pb₁₀Se_{90-x}Ge_x films ($x = 0, 2.5, 5.0, 7.5$ and 10.0 at %) thin films.

Estimated Parameter	a-Pb ₁₀ Se _{90-x} Ge _x thin films (x represents Ge-content at %)				
	$x = 0.0$	$x = 2.5$	$x = 5.0$	$x = 7.5$	$x = 10.0$
λ (Absorption edge, μm)	0.685	0.698	0.698	0.724	0.735
E_o (eV)	3.222	3.161	2.982	2.901	2.879
E_d (eV)	18.182	20.271	21.883	23.359	24.839
$E_d^{(\text{th})}$ (eV)	18.079	18.451	18.850	20.272	20.719
f (eV) ²	58.582	64.077	63.466	67.764	71.511
ϵ_L	6.643	7.413	8.338	9.052	9.784
n_o	2.577	2.723	2.888	3.009	3.128
M_{-1}	5.643	6.413	7.338	8.052	8.628
M_{-3}	0.544	0.642	0.825	0.957	1.041
E_g^{WDD} (eV)	1.611	1.581	1.491	1.451	1.439
E_g^{Tauc} (eV)	1.623	1.601	1.575	1.553	1.538
$E_g^{(\text{th})}$ (eV)	1.566	1.539	1.513	1.486	1.459
(E_o/E_g^{Tauc})	1.985	1.974	1.893	1.868	1.872
ϵ_∞	7.213	7.935	8.956	9.845	10.823
$(N/m^*) \times 10^{53} (\text{g}^{-1} \text{cm}^{-3})$	1.342	1.611	2.016	2.381	2.899
λ_o (nm)	386	393	417	429	447
$S_o \times 10^{13} (\text{m}^2)$	3.792	4.151	4.101	4.379	4.468
$(\alpha_o) \times 10^5 (\text{cm eV})^{-1}$	8.798	7.726	6.416	5.700	5.213
E_e (meV)	61.00	69.00	74.00	82.00	91.00
σ	0.417	0.368	0.343	0.310	0.279
E_{e-p}	3.597	4.076	4.373	4.839	5.376
$\chi^{(1)}$	0.449	0.514	0.584	0.641	0.699
$\chi^{(3)} \times 10^{-12}$ (esu)	4.101	6.789	10.458	17.004	25.553
$n_2 \times 10^{-11}$ (esu)	5.981	9.402	13.822	21.279	30.548
$\omega_p \times 10^{13}$ (Hz)	6.968	7.649	8.541	9.302	10.261
η_{opt}	1.774	1.750	1.724	1.707	1.690

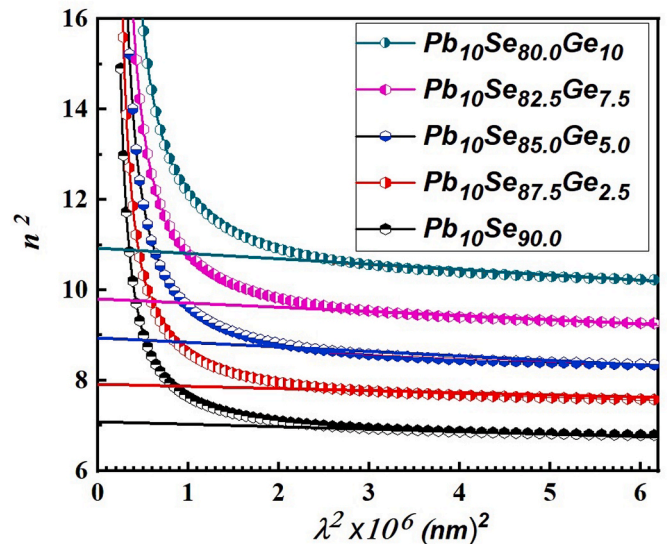


Fig. 7. Illustration of the n^2 Vs λ^2 to get the values of both ϵ_∞ and (N/m^*) of Pb-Se-Ge amorphous film samples.

$(e^2/4\pi^2 c^2 \epsilon_0)(N/m^*)$. The values of both ϵ_∞ and the ratio N/m^* are determined and tabulated in Table 3. The high-frequency dielectric constant value increases with increase in Ge-content and follows the same behavior as that of the lattice dielectric constant (ϵ_L) obtained from the dispersion parameters. The values of the ratio N/m^* are also increasing as the Ge-ratio increases. These computed results match with those obtained by El Nahass, et. at [51].

3.2.4. Sellmeier oscillator wavelength and strength

According to Sellmeier assumption, at higher wavelength or lower frequency of the incident electromagnetic waves, the refractive index (n) can be correlated with the oscillator wavelength (λ_o) and oscillator

strength (S_o) as per following formula [56,57]:

$$\frac{(n_o^2 - 1)}{(n_o^2 - 1)} = 1 - \left(\frac{\lambda_o}{\lambda}\right)^2 \quad (13-a)$$

Rearranging the above Eq., to get:

$$(n^2 - 1)^{-1} = \frac{1}{(n_o^2 - 1)} - \frac{\lambda_o^2}{(n_o^2 - 1)}\lambda^{-2} \quad (13-b)$$

Here, n_o and λ refer to the static index of refraction and the incident wavelength, respectively. ' λ_o ' and ' S_o ' sometimes are called the Sellmeier oscillator parameters and are significant in selection of optical materials for any optical potential application and devices. Sellmeier oscillator parameters can be calculated by using the results obtained from single effective oscillator model.

As ($c = \lambda\nu$) and according to Max Planck's Eq.: $E = h\nu$, therefore, $\lambda = (hc)/(h\nu)$, hence, the last equation can be reformulated to get the following form [13,35,58,59]:

$$(n^2 - 1)^{-1} = \frac{(E_o^2 - (h\nu)^2)}{E_d \times E_o} = \frac{E_o}{E_d} - \frac{(h\lambda)^2}{E_d \times E_o} \quad (14)$$

By comparing these two equations, and by simple modifications, the following equations can be obtained and are elaborately explained in earlier work [13,35,60].

$$E_o = \frac{(hc)}{\lambda_o} \quad \& \quad E_d = (n_o^2 - 1) \frac{(hc)}{\lambda_o} \quad \& \quad S_o = \frac{(n_o^2 - 1)}{\lambda_o^2} \quad (15)$$

Hence, using above equations and the values of both E_o and E_d (Table 3), the wavelength of the oscillator (λ_o) and the strength of the oscillator (S_o) are estimated and are tabulated in Table 3. Moreover, the values of λ_o and S_o parameters may also be determined graphically by representing the refractive index term $(n^2-1)^{-1}$ on the y-axis versus $(\lambda)^{-2}$ on the x-axis, according to the following equation, which is a reformulation of Eq. (14-b) [13,35,60]:

$$(n^2 - 1)^{-1} = \frac{1}{S_o\lambda_o^2} - \frac{1}{S_o\lambda_o^2} \quad \text{where,} \quad S_o = \frac{(n_o^2 - 1)}{\lambda_o^2} \quad (16)$$

Therefore, the slope is equal to $(1/S_o)$ and the intercept of the y-axis gives $(1S_o\lambda_o^2)$. The graphically deduced values (not represented here) are same as those tabulated in Table 3. It can be observed that the determined values of λ_o increases from 386 nm to 447 nm, while S_o increases from $3.792 \times 10^{13} \text{ m}^2$ to $4.468 \times 10^{13} \text{ m}^2$ as the Ge-percentage increases from 0.00% to 10.00% within the ternary amorphous $\text{Pb}_{10}\text{Se}_{90-x}\text{Ge}_x$ films. The increase in λ_o i.e. oscillator wavelength may be attributed to the redshift of the absorption edge, as depicted in Fig. 2 and Table 3. The strength of the oscillator S_o presumably show an increase due to the increase in the bonding energies as Ge-content increases in the glassy matrix.

3.2.5. Absorption coefficient and absorbance

The absorbance spectra (A) of $\text{Pb}_{10}\text{Se}_{90-x}\text{Ge}_x$ thin films is calculated using a set of Eqs. Suggested by Connell and Lewis equations and the obtained transmission spectra (T), as shown in Fig. 2. These set of Eqs. are given as [61]:

$$A = \frac{B + [B^2 + 2qT_a(1 - R_2R_3)]^{1/2}}{q} \quad (17)$$

Here, $B = (R_1-1)(R_2-1)(R_3-1)$ and $q = 2T_a(R_1R_2 - R_1R_3 - R_1R_2R_3)$. Here R_1 , R_2 , and R_3 represent the reflectance at the mutual interfaces. Where R_1 is the reflectance at the air-film material interface and is determined as: $R_1 = [(1 - n)/(1 + n)]^2$. The reflectance R_2 is that of the film material - glass-substrate interface and computed as follows: $R_2 = [(n - s)/(n + s)]_2$. While R_3 is the reflectance at the glass substrate-surrounding air interface and is calculated as: $R_3 = [(s - 1)/(s_2(1 +$. Therefore, the absorption coefficient, α can be determined as follows

[62,63]:

$$A = \exp(\alpha \times d) \quad (18)$$

Here, (d) is film thickness and (A) is the absorbance. The obtained absorption coefficient (α) values are represented as a function of the photon energy ($h\nu$) in Fig. 8. The absorption coefficient has the values of the order of 10^4 cm^{-1} .

Moreover, it decreases sharply as the photon energy decreases, reaching very quickly to zero. The (α) value increases as Ge-content increases. This behavior was observed for many semiconducting films, either for similar film materials or different materials [51,52,64,65]. As shown also in Fig. 8, the absorption edge of film samples is shifted towards lower energy values, completely consistent with Fig. 2.

This redshift in the absorption edge is due to the addition of germanium on the account of Se . Therefore, it can be said that the Ge-addition increases the sample's absorbance capability of the incident light. The absorption edge wavelength or energy has a great significance in investigating the electronic transitions of the semiconducting materials, along with the knowledge of the energy band structure of the material [51]. The absorption edge wavelength values are reported in Table 3.

3.2.6. Optical band-gap and Urbach energies

In semiconducting materials as suggested by Tauc [66,67] and further developed by Mott and Davis [68], the energy required for an electron to jump and transit the forbidden band gap depends on both the intrinsic behavior of the material and the incident photon energy ($h\nu$) [66-68]. The energy required for an electronic transition from VB to CB is defined as the optical band-gap energy (E_g) or bandgap width. The absorption strength of the incident electromagnetic waves for any semiconducting materials is usually dependent on the difference between the band-gap energy (E_g) and incident photon energy ($h\nu$).

The optical band gap is calculated using absorption coefficient values as a function of wavelength using Tauc's relation [66-68]:

$$(\alpha h\nu) = \alpha_o (h\nu - E_g)^p \quad (19)$$

Where $h\nu$ is the photon energy and (α) is absorption coefficient. The parameter (α_o) is called the band-tailing parameter; it depends on the semiconductor material and its optical absorption ability, as well as the type of the electronic transition [35,59]. The value of the exponent power factor $p = \frac{1}{2}$ and 2 for direct and indirect transitions, respectively [59,69]. For the material under investigation, $p = 2$. While plotting a

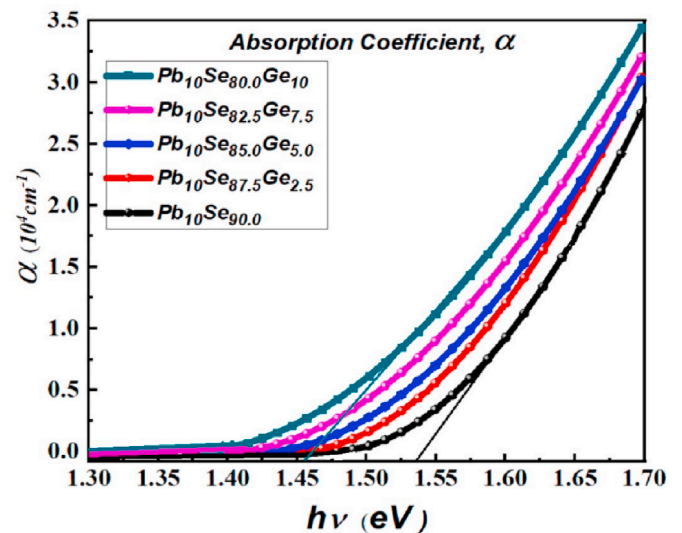


Fig. 8. The variation of the absorption coefficient spectra of the amorphous Pb-Se-Ge films.

graphical relationship between $(h\nu)$ on the horizontal axis and $(\alpha h\nu)$ on the vertical axis (to check the possible p -values) the straight line is obtained for $p = 2$. This hints towards the indirect allowed transitions.

The graphical relationship between $(\alpha h\nu)^{1/2}$ versus $(h\nu)$ is plotted, and the line has been extrapolated to intersect the x-axis at a certain point. This point depicts optical gap energy value for the present a-Pb₁₀Se_{90-x}Ge_x films. Fig. 9 represents this graphical representation, and therefore the energy of the optical band gap is experimentally inferred for the film samples. This verification for Tauc's Eq., for Pb–Se–Ge thin films, is consistent with what Mott and Davis suggested for the non-crystalline materials. Where they proposed that the electronic transition of the amorphous semiconductor material is almost an indirect allowed transition, which was affirmed for the present film samples. Consequently, Eg(Tauc)-values have been obtained and then reported also in Table 3.

It can see that the value of the optical bandgap energy of Pb₁₀Se_{90-x}Ge_x films decreases from 1.623 eV to 1.538 with an increase in Ge-content from $x = 0.00\%$ to $x = 10.0\%$. In the present manuscript, authors have computed the optical energy gap using more than one method, using the single effective oscillator model, E_g^{WDD} and theoretically, $E_g^{(th)}$ using Shimakawa's formula [23,70]. The band-gap values obtained from these three methods are very close to each other follows the same trend. This indicates the high accuracy of the computations done.

Furthermore, Fig. 11-a, b and c show the graphical representation of the optical energy gap values as functions of the Ge-content, corresponding to the obtained values by WDD model, Tauc's Plot and calculated theoretically. Fig. 11-a illustrates the determined optical band energy values according to Tauc's plot, $E_g^{(Tauc)}$ and the results plotted as a function of (x) atomic %, which denotes to the Ge-content percentages, then the points are linearly fitted to obtain the following experimental equation: $E_g^{(Tauc)}(eV) = 1.623 - 0.009x$.

The Ge-addition results in the generation of more localized states/band tail within the band gap. This band tail leads to a decrease in the bandgap width, hence decreases E_g -values. This result matches the results presumed by Tanaka (1980) and by Kato and Tanaka (2005) [46, 71]. It is worth noticing that the pre-exponential values of Eq. (20), α_0 is also estimated for the present films (Table 3), and is found to decrease from 8.798×10^5 (cm eV)⁻¹ to become 5.213×10^5 (cm eV)⁻¹, as Ge-content increases from 0.00% to 10.0%. Moreover, it can also be noted that α_0 -values shows the same behavior as that of the optically obtained band-gap energy (E_g), where the two values decrease together as Ge-ratio increases. While the two quantities (α_0 and E_g) are in an

inverse relationship with the refractive index values (refer to Tables 2 and 3).

These obtained results affirm that the non-crystalline Pb₁₀Se_{90-x}Ge_x films have the behavior of semiconductor materials [24,35,39]. As the authors' knowledge, either (the direct relationship between α_0 and E_g) or (the inverse relationship between α_0 and n) has not been previously discussed or touched by anyone, and therefore the authors have not found any reference that can be cited here to confirm this relationship or essentially deny it. Nevertheless, authors have noticed this behavior previously as well [35] and therefore can be considered as a note.

Urbach stated that along the curve of the optical absorption coefficient (α -spectra) of the semiconductors and almost near the absorption-edge of amorphous, or polycrystalline semiconducting materials, there is an exponential segment [69] which describes the width of the band-tail of semiconductor materials. This tail exemplifies the localized states. According to Urbach [72]:

$$\alpha = \beta_0 \exp\left(\frac{h\nu}{E_e}\right) \quad (20)$$

Where β_0 is some constant, E_e is the band-tail. A straight-line near the absorption edge is obtained while plotting $\ln(\alpha)$ vs photon energy ($h\nu$) and the reciprocal of the slope gives the value of E_e , as illustrated in Fig. 10.

The values of the band-tail energies have been reported in Table 3 and graphically depicted as a function of the percentage values of Ge-content in Fig. 11-d. The represented graphical points have been also fitted to get this empirical Eq.:

$$E_e(\text{meV}) = 60.96 + 2.99x, \quad x = 0.0, 2.5, 5.0, 7.5, \text{ and } 10.0 \text{ At.}\%$$

As obvious from this graph and Table 3, the band-tail width energy increases from 61 meV to 91 meV. This means that the disordered of the non-crystalline Pb₁₀Se_{90-x}Ge_x matrix increases as Ge- increase in the system. Thereby, the localized states width, formed above and below of the VB and CB, respectively increase. These results confirm the obtained results of the band-gap energies and are in a good match with similar chalcogenide film samples [45,51,52].

On the other side, Urbach assumed another hypothesis for the amorphous semiconductors that linked between the energy of the band-tail-width (or the formed localized states) and the coefficient of the absorption, α of these materials, according to this expression [72–74]:

$$\alpha = \mu \exp\left[\frac{\sigma(h\nu - E_c)}{KT}\right] \quad (21)$$

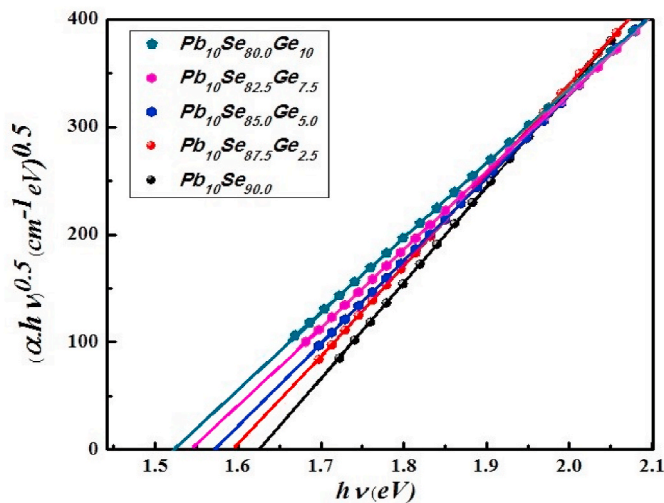


Fig. 9. Absorption curves illustrating the indirect allowed transition and obtaining the optical band-gap energy, E_g (Tauc) of the a-Pb₁₀Se_{90-x}Ge_x thin film samples.

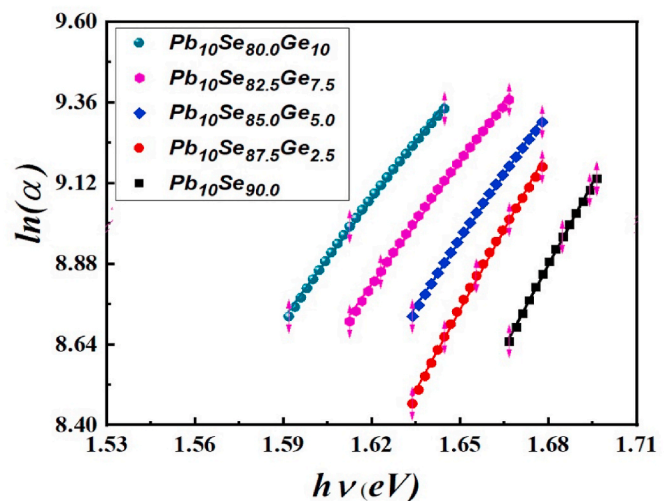


Fig. 10. Illustrating $\ln(\alpha)$ Vs $(h\nu)$ to get the Urbach band-tail energy E_U of the ternary Pb–Se–Ge film samples.

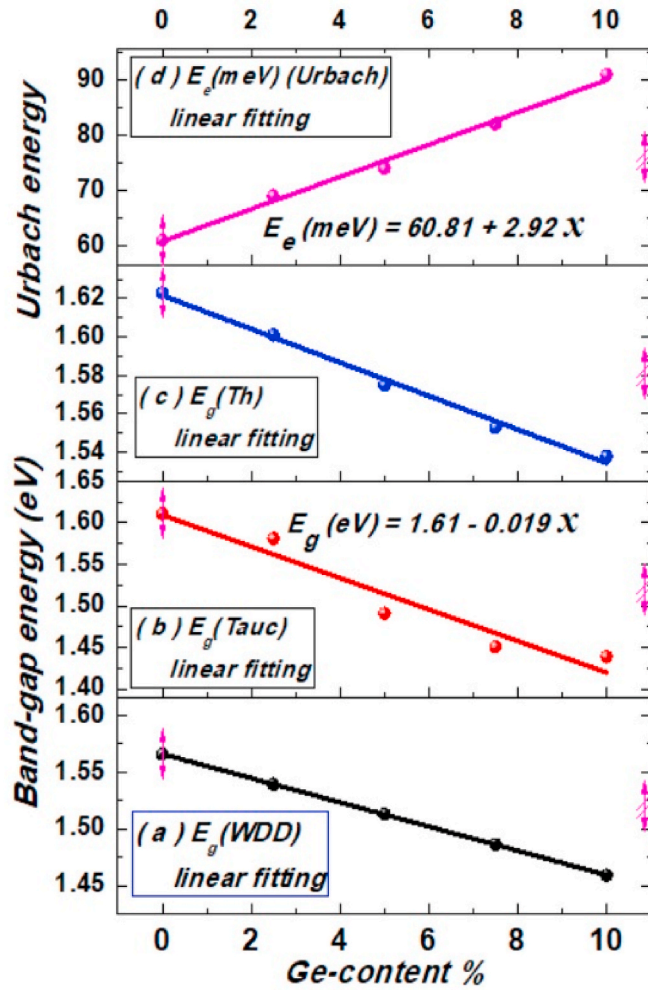


Fig. 11. Representation of the $E_g(\text{WDD})$, $E_g(\text{Tauc})$, $E_g(\text{Th})$ and E_e as functions of the Ge-content % of the ternary a-Pb₁₀Se_{90-x}Ge_x thin films.

Here, (μ) is another constant, differs from β_o , that of Eq. (21), while (σ) is steepness parameter, and T is the absolute room temperature, 295 K [73,74]. This parameter also characterizes the broadening of the edge. μ characterizes the slope of the straight portion of the absorption coefficient curve (α) or/and the absorbance (A) near the edge of the absorption. As E_o is the energy of the electronic transition. $E_o = E_g + E_p$, where E_p is the energy of the phonon accompanying the indirect electronic transition, whereas for the allowed direct transition, $E_o = E_g$, and the constant K denotes Boltzmann constant.

Therefore, from the comparison of the two Eqs. (20) and (21), it can get these Eqs. [37,69,72,74]:

$$\ln(\alpha_o) = \left(\ln \beta - \frac{\sigma E_o}{KT} \right) \quad \text{and} \quad \frac{(\hbar\nu)}{E_e} = \frac{\sigma(\hbar\nu)}{KT} \quad (22\text{-a})$$

$$\text{Consequently : } \sigma = \frac{KT}{E_e} \quad (22\text{-b})$$

Thus, the value of this steepness parameter (σ) is computed and is given in Table 3. It was found that the values of the steepness parameter decrease from 0.417 to 0.279 with the increase of the Ge-percentage in the film sample. This means the broadening of the absorption edge decreases as Ge-content increased, i.e. the interactions of the electron-phonon and/or the exciton-phonon increases [75,76]. Where the steepness parameter (σ) is related to the strength of the electron-phonon interactions, E_{e-p} by the following Eq. [37,69]:

$$E_{e-p} = 3 / (2\sigma) \quad (23)$$

Therefore, the electron-phonon interaction strength, E_{e-p} could be also evaluated and then reported in Table 3. The value of E_{e-p} increased from 3.597 to 5.376, as the Ge-ratio increased from 0.0% to 10.0%.

3.2.7. Non-linear optical parameters

The optical nonlinearity of the refractive index is connected with the high-order susceptibility of the material. When applying a strong electric field to a substance (when an intensive light incident on the material), then the material will be polarized. This polarization (P) and the applied electric field, E can be described as follows [77,78]:

$$P = \chi^{(1)}E + \chi^{(2)}E^2 + \chi^{(3)}E^3 \quad (24)$$

Where $\chi^{(1)}E$ is linear and while $\chi^{(2)}$ and $\chi^{(3)}$ represent the higher order nonlinear susceptibilities. Further, the refractive index 'n' can also be given as follows [78–81]:

$$n = n_o + n_2(E^2) \quad (25)$$

Noting that (n_o) and (n_2) are independent of the intensity of the incident light and $n_o \gg n_2$. Using Miller's rule, the first-order and third-order nonlinear susceptibilities, ($\chi^{(1)}$) and ($\chi^{(3)}$), respectively, and nonlinear refractive index (n_2) of any semiconducting material is determined as following set of Eqs. [45,79–82]:

$$\chi^{(1)} = \frac{\eta_o^2 - 1}{4\pi} \quad (26)$$

$$\chi^{(3)} = \frac{B}{(4\pi)^4} [\eta_o^2 - 1]^4 \quad (27)$$

$$\eta_2 \cong \frac{C}{E_g^4} \quad (28)$$

Here, n_o is the obtained static refractive index, B and C are constants and equal 1.7×10^{-10} (esu) and 1.26×10^{-9} (esu.(eV)⁴), respectively. These Eqs. 26–28 give sensible values as predicted by Ticha and Tichy (2002) [79]. Thus, by substituting the values of n_o and the mentioned constants (B and C), the values of both $\chi^{(1)}$, $\chi^{(3)}$ and n_2 values can be computed, and then listed in Table 3. As obvious, these three parameters ($\chi^{(1)}$, $\chi^{(3)}$ and n_2) are increasing as the Ge-percentage increases, due to the increase in the values of n_o , which is dependent upon the E_d/E_o ratio, which is also increasing and discussed before [79–81].

3.2.8. The plasma frequency, ω_p and optical electronegativity, η_{opt}

The plasma frequency (ω) has an essential function in the absorption of incident electromagnetic waves. The frequency of the electromagnetic waves (photons), ($\hbar\nu$) has the same order of the plasma frequency (ω_p) and leads to a large absorption of light owing to the coupling between photons and phonons. This coupling affects the values of the bandgap energy (E_g) and the index of refraction (n) [78]. If the frequencies of both the photon and the phonon become equal, then an anomalous dispersion of the index of refraction occurs in the plasma region of the material. As the energy of the incident light increases, the refractive index (n)-values and the absorption of incident light increase, which further slows down the speed of electromagnetic waves within the materials [35]. Due to these significant effects of the plasma frequency, it can be calculated as follows [35,80–83]

$$\frac{N}{m^*} = \frac{\epsilon_0 \epsilon_\infty \omega_p^2}{e^2} \quad \text{or} \quad \omega_p^2 = \frac{N}{m^*} \times \frac{e^2}{\epsilon_0 \epsilon_L} \quad (29)$$

Consequently, the values of ω_p have been determined and listed in Table 3. As it is seen the value of this frequency, ω_p increases from 6.968×10^{13} Hz to 10.261×10^{13} Hz. This means that the increase in the Ge-content leads to the increase in the plasma frequency.

On the hand, the optical electronegativity, (η_{opt}) is another

parameter which has a crucial role in estimating several parameters from the Physico-chemical characteristics of the materials as suggested by Duffy [84]. It physically means that the tendency of a radical or ion to attract electrons for forming the ionic bond. The values of the optical electronegativity for any chalcogenide amorphous SCM can be calculated by the following Eq. [84,85]:

$$\eta_{opt} = \left[\frac{A}{n_0} \right]^{1/4} \quad (30)$$

Here, A denotes a constant for all materials, which is a dimensionless quantity, it equals 25.54. Thus, the optical electronegativity values could be determined and then reported in Table 3. It can be observed that the value of η_{opt} decreases from 1.774 to 1.690 as the Ge- ratio increases from 0.00% to 10.0% in the chalcogenide amorphous $Pb_{10}Se_{90-x}Ge_x$ films.

4. Conclusion

The amorphous $Pb_{10}Se_{90-x}Ge_x$ ($x = 0.00, 2.50, 5.00, 7.50$ and 10.00 at. %) thin films have been synthesized using the vacuum deposition under pressure about 5×10^{-4} Pa. The optical properties or parameters of the prepared thin films have been studied using optical transmission measurements and Swanepoel envelop method. The films have strong absorption between 700 nm and 900 nm, and the absorption edge of films shows a red-shift from 683 nm to 735 nm, approximately as the Ge-content increases. After 900 nm the absorbing nature of thin films reduces to a minimum value to then approach zero. An increase in the Ge-content leads to an increase in the refractive index values of samples. WDD Model is employed to deduce the dispersion energies and parameters. Moreover, Sellmeier oscillator wavelength and strength are also determined and discussed. The absorption coefficient spectra is higher than 10^{-4} cm^{-1} . Tauc's and Urbach's energies are investigated and thoroughly discussed. The electronic transition is indirect, and energy of the optical bandgap decreases from 1.623 eV to 1.538 eV, while the Urbach energy increases from 61 meV to 91 meV with an increase in Ge content. The bonding strength and the cohesive energy of samples strongly affect the optical properties and parameters. Moreover, all discussed characteristics and parameters strongly depends upon the Ge-concentration. The effective single oscillator energy and the optical electronegativity decreases. While almost all the other estimated parameters increase, viz. the dispersion energy, oscillator strength, lattice dielectric constant, the static refractive index, the moments (M_1 and M_3), oscillator wavelength, Steepness constant, plasma frequency and the nonlinear optical parameters ($\chi^{(1)}$, $\chi^{(3)}$ and n_2).

Funding

This research was not funded by any authority, the authors bear all the costs of the work.

Credit author statement

Ahmed Saeed Hassanien, Conceptualization, Methodology, Formal analysis, Writing, Writing – original draft, Investigation, Supervision, Project administration, Resources, Visualization. Ishu Sharm, Idea, Formal analysis, Writing, Writing – review & editing, Project administration, Resources, Validation, Visualization. Kamal A. Aly, Methodology. Formal analysis, Data curation, Project administration, Resources, Software, Validation.

Declaration of competing interest

The authors declare that they have no conflict of interest.

References

- [1] Panpan Guo, Chengdong Li, Wei Huang, Wei Zhang, Peiqing Zhang, Tiefeng Xu, Thermal annealing of Ge-Se thin films and its influence on waveguide performance, *Opt. Mater. Express* 10 (1) (2020) 129–137.
- [2] Yongsheng Hu, Kangzhen Tian, Tongtong Li, Mingjie Zhang, Ren He, Sisheng Qi, Anping Yang, Xian Feng, Zhiyong Yang, Mid-infrared nonlinear optical performances of Ge-Sb-S chalcogenide glasses, *Opt. Mater. Express* (2021) 695–706, 11.
- [3] Hao Xiong1, Zheyao Wang, Fabrication of ternary Ge–Se–Sb chalcogenide microlens arrays using thermal reflow, *J. Micromech. Microeng.* 29 (2019) 8, 085002.
- [4] A.S. Hassanien, A.A. Akl, Influence of thermal and compositional variations on conduction mechanisms and localized state density of amorphous $Cd_{50}S_{50-x}Se_x$ thin films, *J. Non-Cryst. Solids* 487 (2018) 28–36.
- [5] J.L. Adam, X. Zhang, *Chalcogenide Glasses: Preparation, Properties and Applications*, first ed., Elsevier Science, ScienceDirect, 2014.
- [6] Xusheng Xiao, Yantao Xu, Jian Cui, Xiaogang Liu, Xiaoxia Cui, Xunsi Wang, Shixun Dai, Haitao Guo, Structured active fiber fabrication and characterization of a chemically high-purified Dy^{3+} -doped chalcogenide glass, *J. Am. Ceram. Soc.* 103 (4) (2020) 2432–2442.
- [7] A.S. Hassanien, I.M. El Radaf, A.A. Ak, Physical and optical studies of the novel non-crystalline $Cu_xGe_{20-x}Se_{40}Te_{40}$ bulk glasses and thin films, *J. Alloys Compd.* 849 (2020) 156718.
- [8] A.S. Hassanien, A.A. Akl, Estimation of some physical characteristics of chalcogenide bulk $Cd_{50}S_{50-x}Se_x$ glassy systems, *J. Non-Cryst. Solids* 428 (2015) 112–120.
- [9] Pawan Kumar, S.K. Tripathi, Ishu Sharma, Effect of Bi addition on the physical and optical properties of $Ge_{20}Te_{74-x}Sb_6Bi_x$ ($x = 2, 4, 6, 8, 10$) thin films deposited via thermal evaporation, *J. Alloys Compd.* 755 (2018) 108–113.
- [10] Abdelkader Medjouri, Djamel Abed, Mid-infrared broadband ultraflat-top supercontinuum generation in dispersion engineered Ge-Sb-Se chalcogenide photonic crystal fiber, *Opt. Mater.* 97 (2019) 109391.
- [11] I. Sharma, Temperature-dependent photoconductive properties of Ge-Sb-Te thin films, *Phase Transitions* 92 (9) (2019) 851–861.
- [12] A.S. Hassanien, I. Sharma, Optical properties of quaternary a- $Ge_{15-x}Sb_xSe_{50}Te_{35}$ thermally evaporated thin-films: refractive index dispersion and single oscillator parameters, *Optik* 200 (2020) 163415.
- [13] A.A. Akl, A.S. Hassanien, Microstructure and crystal imperfections of nanosized $CdS_{50}Se_{1-x}$ thermally evaporated thin films, *Superlattice. Microsc.* 85 (2015) 67–81.
- [14] E.A. Romanova, Yu.S. Kuzutkina, V.S. Shiryayev, S. Guizard, Investigation of the dynamics of a nonlinear optical response in glassy chalcogenide semiconductors by the pump – probe method, *Quant. Electron.* 48 (3) (2018) 228–234.
- [15] Jixing Liu, Shengnan Zhang, Lina Sang MengLi, Weiyao Zhao, ZhiLi, Zhenxiang Cheng, Liqiang Liu, Botao Shao, Jianqing Feng, Chengshan Li, Pingxiang Zhang, Shixue Dou, Xiaolin Wang, Lian Zhou, Boosting the superconducting properties of Fe(Se, Te) through hexagonal phase manipulation, *J. Alloys Compd.* 816 (5) (2020) 152683.
- [16] A.S. Hassanien, A.A. Akl, X-Ray Studies, CO_2 pulsed laser annealing effects crystallography, microstructure and crystal defects vacuum deposited nanocrystalline ZnSe thin films, *CrystEngComm* 20 (2018) 7120–7129.
- [17] A.S. Hassanien, I. Sharma, A.A. Akl, Physical and optical properties of a-Ge-Sb-Te bulk and film samples: refractive index and its association with electronic polarizability of thermally evaporated a- $Ge_{15-x}Sb_xSe_{50}Te_{35}$ thin-films, *J. Non-crystalline Solids* 531 (2020) 119853.
- [18] I. Sharma, A. Kumar, S.K. Tripathi, P.B. Barman, Effect of Bi addition on the electrical properties of a-Ge–Se–In thin films, *J. Physics D:Applied Physics* 41 (2008) 17, 175504.
- [19] S. Murugavel, S. Asokan, Carrier-type reversal in Pb-modified chalcogenide glasses, *Phys. Rev. B* 58 (1998) 4449.
- [20] A.S. Hassanien, I. Sharma, Band-gap engineering, conduction and valence band positions of thermally evaporated amorphous $Ge_{15-x}Sb_xSe_{50}Te_{35}$ thin films: influences of Sb upon some optical characterizations and physical parameters, *J. Alloys and compounds* 798 (2019) 750–763.
- [21] P. Kumar, J. Kaur, S.K. Tripathi, I. Sharma, Effect of antimony (Sb) addition on the linear and non-linear optical properties of amorphous Ge–Te–Sb thin films, *Indian Journal of Physics*, *Indian journal of physics* 91 (12) (2017) 1503–1511.
- [22] Balbir Singh Patial, Neha sharma, Nagesh Thakur, Structural analysis and theoretical investigations in Pb additive Se-Te-Ge chalcogenide nano-composites, *Indian J. Pure Appl. Phys.* 56 (2) (2018) 128–135.
- [23] M. Kang, L. Sisken, C. Lonergan, A. Buff, A. Yadav, C. Goncalves, C. Blanco, P. Wachtel, J.D. Musgraves, A.V. Pogrebnaykov, E. Baleine, C. Rivero-Baleine, T. S. Mayer, C.G. Pantano, K.A. Richardson, Monolithic chalcogenide optical nanocomposites enable infrared system innovation, *Gradient Refractive Index Optics* 8 (10) (2020), 2000150. *Advanced Optical Materials*.
- [24] K. Petkov, J. Tasseva, V. Vassilev, L. Aljihmani, Compositional dependence of the optical properties of vacuum evaporated thin $GeSe_2$ - $GeTe$ - $PbTe$ films *Physics, Procedia* 44 (2013) 130–141.
- [25] S.A. Fayek, M.M. El-Ocker, A.S. Hassanien, Optical and electrical properties of $Ge_{10+x}Se_{40}Te_{50-x}$ thin film, *Mater. Chem. Phys.* 70 (2) (2001) 231–235.
- [26] R.T. Ananth Kumar, N. Qamhi, Saleh T. Mahmoud, Electrical and crystallization properties of indium doped Ge-Sb-Se films, *J. Alloys Compd.* 768 (2018) 817–823.
- [27] K. Petkov, J. Tasseva, V. Vassilev, L. Aljihmani, Compositional dependence of the optical properties of vacuum evaporated thin $GeSe_2$ - $GeTe$ - $PbTe$ films *Physics, Procedia* 44 (2013) 130–141.

- [28] P. Sharma, Glass-forming ability and rigidity percolation in SeTePb lone-pair semiconductors, *Appl. Phys. A* 122 (2016) 402.
- [29] David R. Lide (Ed.), CRC Handbook of Chemistry and Physics, 88th edition, Taylor & Francis Group, Boca Raton, Florida, 2008.
- [30] L. Pauling, The Nature of the Chemical Bond, third ed., Cornell University Press, Ithaca, NY, 1960.
- [31] Samuel Ruben, Handbook of the Elements, January, vol. 8, Open Court Publishing Company, La Salle, Illinois, 1999, p. 61301.
- [32] R. Swanepoel, Determination of surface roughness and optical constants of inhomogeneous amorphous silicon films, *J. Phys. E Sci. Instrum.* 17 (10) (1984) 896–903.
- [33] R. Swanepoel, Determination of the thickness and optical constants of amorphous silicon, *J. Phys. E Sci. Instrum.* 16 (12) (1983) 1214–1222.
- [34] K.A. Aly, F.M. Abdel-Rahim, Effect of Sn addition on the optical constants of Ge–Sb–S thin films based only on their measured reflectance spectra, *J. Alloys Compd.* 561 (2013) 284–290.
- [35] A.S. Hassanien, R. Neffati, K.A. Aly, Impact of Cd-addition upon optical properties and dispersion parameters of thermally evaporated $Cd_xZn_{1-x}Se$ films: discussions on bandgap engineering, conduction and valence band positions, *Optik* 212 (2020) 164681.
- [36] D.J. Borah, A.T.T. Mostako, P.K. Saikia, P. Dutta, Effect of thickness and post deposition annealing temperature on the structural and optical properties of thermally evaporated molybdenum oxide films, *Mater. Sci. Semicond. Process.* 93 (2019) 111–122.
- [37] A.S. Hassanien, A. Akl Alaa, Optical characteristics of iron oxide thin films prepared by spray pyrolysis technique at different substrate temperatures, *Appl. Phys. A* 124 (2018) 752.
- [38] I. Sharma, A.S. Hassanien, Effect of Ge-addition on physical and optical properties of chalcogenide $Pb_{10}Se_{90-x}Ge_x$ bulk glasses and thin films, *J. Non-Cryst. Solids* 548 (2020) 120326.
- [39] A.S. Hassanien, K.A. Aly, A.A. Akl, Study of optical properties of thermally evaporated ZnSe thin films annealed at different pulsed laser powers, *J. Alloys Compd.* 685 (2016) 733–742.
- [40] Pankaj Sharma, K.A. Aly Dahshan, New quaternary Ge–Se–Sb–Ag optical materials: blue shift in absorption edge and evaluation of optical parameters, *J. Alloys Compd.* 616 (2014) 323–327.
- [41] J.C. Manifacier, J. Gasiot, J.P. Fillard, A simple method for the determination of the optical constants n , k and the thickness of a weakly absorbing thin film, *J. Phys. (Paris)* 9 (11) (1976) 1002.
- [42] M. Mohamed, E.R. Shaaban, M.N. Abd-el Salam, A.Y. Abdel-Latifa, S. A. Mahmoud, M.A. Abdel-Rahim, Investigation of the optical and electrical parameters of $As_{47.5}Se_{47.5}Ag_5$ thin films with different thicknesses for optoelectronic applications, *Optik* 178 (2019) 1302–1312.
- [43] A. Dahshan, H.H. Amer, K.A. Aly, Compositional dependence of the optical constants of amorphous $Ge_xAs_{20}Se_{80-x}$ thin films, *J. Phys. D Appl. Phys.* 41 (2008) 7, 215401.
- [44] K.A. Aly, Optical band gap and refractive index dispersion parameters of $As_xSe_{70}Te_{30-x}$ ($0 \leq x \leq 30$ at. %) amorphous films, *Appl. Phys. A* 99 (2010) 913.
- [45] P. Sharma, K.A. Aly, Dinesh Ch Sati, A. Dahshan, Improvement in the linear and nonlinear optical properties of Mn-doped $GeSe_2$ chalcogenide thin films for all optical applications, *Appl. Phys. A* 126 (2020) 173.
- [46] K. Tanaka, Optical properties and photoinduced changes in amorphous As-S films, *Thin Solid Films* 66 (1980) 271–279.
- [50] S.H. Wemple, M. DiDomenico, Optical dispersion and the structure of solids, *physical review letter* 23, 193, Erratum *Phys. Rev. Lett.* 24 (1969) 1156, 1970.
- [51] M.M. El-Nahass, M.B. El-Den, H.M. El-Mallah, F.S. Abu-Samaha, Effects of Pb addition and heat treatment on optical properties of thermally evaporated $Ge_{1-x}Se_2Pb_x$ thin films, *J. Phys. Chem. Solid.* 69 (2008) 2652–2659.
- [52] Hukam Singh Deepika, N.S. Saxena, Optical properties of nanostructured $Se_{58}Ge_{39}Pb_3$ and $Se_{58}Ge_{36}Pb_6$ thin films, national conference on advanced materials and nanotechnology, AIP Conf. Proc. (2018) 2009, <https://doi.org/10.1063/1.5052088>, 20019-1–020019-4.
- [53] S.H. Wemple, M. DiDomenico, Behavior of the Electronic Dielectric Constant in Covalent and Ionic Materials *Physical Review B*, vol. 3, 1971, p. 1338.
- [54] S.H. Wemple, Refractive-index behavior of amorphous semiconductors and glasses, *Phys. Rev. B* 7 (1973) 3767.
- [55] F.A. Jenkins, H.E. White, *Fundamentals of Optics*, McGraw-Hill, New York, 1957.
- [56] V. Brückner, To the Use of Sellmeier Formula, HFT Leipzig, Germany, 2011 (SES) Bonn.
- [57] W. Sellmeier, To explain the abnormal colour sequence in the spectrum of some substances, *Ann. Phys.* 143 (1871) 272–282.
- [58] A.K. Walton, T.S. Moss, Determination of refractive index and correction to effective electron mass in PbTe and PbSe, *Proc. Phys. Soc.* 81 (1963) 509–513.
- [59] A.S. Hassanien, A.A. Akl, Influence of composition on optical and dispersion parameters of thermally evaporated non-crystalline $Cd_{50}S_{50-x}Se_x$ thin films, *J. Alloys Compd.* 648 (2015) 280–290.
- [60] A.S. Hassanien, A.A. Akl, Optical characterizations and refractive index dispersion parameters of annealed TiO_2 thin films synthesized by RF-sputtering technique at different flow rates of the reactive oxygen gas, *Phys. B Condens. Matter* 576 (2020) 411718.
- [61] G.A.N. Connell, A.J. Lewis, Comments on the evidence for sharp and gradual optical absorption edges in amorphous germanium, *Phys. Status Solidi* 60 (1973) 291.
- [62] K.A. Aly, Optical band gap and refractive index dispersion parameters of $As_xSe_{70}Te_{30-x}$ ($0 \leq x \leq 30$ at. %) amorphous films, *Appl. Phys. Mater. Sci. Process* 99 (2010) 913–919.
- [63] K.A. Aly, S.R. Alharbi, Y.B. Saddeek, A. Mossad Ali, A. Dahshan, Kh.S. Shaaban, Physical characterization of As-Se-S glasses, *Mater. Res. Express* 5 (2018), 065208.
- [64] I.M. El Radaf, H.Y.S. Al-Zahrani, A.S. Hassanien, Novel Synthesis, structural, linear and nonlinear optical properties of p-type kesterite nanosized Cu_2MnGeS_4 thin films, *J. Mater. Sci. Mater. Electron.* 31 (2020) 8336–8348, <https://doi.org/10.1007/s10854-020-03369-9>.
- [65] A.S. Hassanien, I.M. El Radaf, Optical characterizations of quaternary Cu_2MnSnS_4 thin films: novel synthesis process of film samples by spray pyrolysis technique, *Physica B* 585 (2020) 412110.
- [66] J. Tauc, Optical properties and electronic structure of amorphous Ge and Si, *Mater. Res. Bull.* 3 (1968) 37–46.
- [67] J. Tauc, in: J. Tauc (Ed.), *Amorphous and Liquid Semiconductors*, Plenum Press, London and New York, 1974.
- [68] E.A. Davis, N.F. Mott, Conduction in non-crystalline systems V. Conductivity, optical absorption and photoconductivity in amorphous semiconductors, *Philos. Mag. A* 22 (179) (1970) 903–922.
- [69] A.S. Hassanien, A.A. Akl, Effects of Se on optical and electrical properties of chalcogenide $CdSs$ thin films, *Superlattice. Microst.* 89 (2016) 153–169.
- [70] M. Askari, N. Soltani, E. Saion, W.M. Mat Yunus, H.M. Erfani, M. Dorostkar, Structural and optical properties of PVP-capped nanocrystalline $Zn_xCd_{1-x}S$ solid solutions, *Superlattice. Microst.* 81 (2015) 193–201.
- [71] T. Kato, K. Tanaka, Electronic properties of amorphous and crystalline $Ge_2Sb_2Te_5$ films, *Jpn. J. Appl. Phys.* 44 (10) (2005) 7340–7344.
- [72] F. Urbach, The long-wavelength edge of photographic sensitivity and of the electronic absorption of solids, *Phys. Rev.* 92 (1953) 1324.
- [73] G.V. Makhnovets, G.L. Myronchuk, L.V. Piskach, B.V. Vidrynskyi, A.H. Kevshyn, Study of optical absorption in $TiGaSe_2:Zn^{2+}$ single crystals, *Ukr. J. Phys. Opt.* 19 (1) (2018) 49–59.
- [74] I. Studeniyak, M. Kranjec, M. Kurik, Urbach rule in solid state physics, *Int. J. Opt. Appl.* 4 (3) (2014) 76–83.
- [75] A. Abu El-Fadl, A.S. Soltan, N.M. Shaalan, Temperature dependence of the indirect band gap, steepness parameter and related optical constants of $[K_x(NH_4)_{1-x}]_2ZnCl_4$ mixed crystals, *Opt Laser. Technol.* 39 (2007) 1310–1318.
- [76] T. Skettrup, Urbach's rule derived from thermal fluctuations in the band-gap energy, *Phys. Rev. B* 18 (1978) 2622.
- [77] D.C. Sati, S.C. Katyal, P. Sharma, Role of composition and substrate temperature on nonlinear optical properties of $GeSeTe$ thin 0.4–2.4- μm wavelength range, *IEEE Trans. Electron. Dev.* 63 (2016) 698–703.
- [78] E. Sharma, P.B. Barman, Pankaj Sharma, Evaluation of optical linear and non-linear parameters of thermally deposited $GeTeSeGa$ thin films in NIR (1 μm –2.6 μm) wavelength range from their transmission spectra, *Optik* 219 (2020) 165181.
- [79] H. Ticha, L. Tichy, Semiempirical relation between non-linear susceptibility (Refractive index), linear refractive index and optical gap and its application to amorphous chalcogenides, *J. Optoelectron. Adv. Mater.* 4 (2002) 381–386.
- [80] A.S. Hassanien, Studies on dielectric properties, opto-electrical parameters, and electronic polarizability of thermally evaporated amorphous $Cd_{50}S_{50-x}Se_x$ thin films, *J. Alloys Compd.* 671 (2016) 566–578.
- [81] E. Sharma, P.B. Barman, P. Sharma, Evaluation of optical linear and non-linear parameters of thermally deposited $GeTeSeGa$ thin films in NIR (1 μm –2.6 μm) wavelength range from their transmission spectra, *Optik* 219 (2020) 165181.
- [82] A.S. Hassanien, H.R. Alamri, I.M. El Radaf, Impact of film thickness on optical properties and optoelectrical parameters of novel $CuGaGeSe_4$ thin films synthesized by electron beam deposition, *Opt. Quant. Electron.* 52 (2020) 335, <https://doi.org/10.1007/s11082-020-02448-9>.
- [83] A.A. Al-ghamdia, H. Alhummiyanb, M.Sh Abdel-wahaba, I.S. Yahia, Structure, optical constants and non-linear properties of high-quality AZO nano-scale thin films, *Optik* 127 (2016) 4324–4328.
- [84] J.A. Duffy, Trends in energy gaps of binary compounds: an approach based upon electron transfer parameters from optical spectroscopy, *J. Phys. C Solid State Phys.* 13 (1980) 2979–2989.
- [85] J.A. Duffy, *Bonding Energy Levels and Bonds in Inorganic Solids*, Longman Scientific and Technical, England, 1990.